JOURNAL OF MATERIALS SCIENCE 24 (1989) 2643–2652

Properties of elongational flow injection moulded polyethylene

Part 3 *Influence of molecular weight*

R. K. BAYER*, F. J. BALTÁ CALLEJA
Instituto de Estructura de la Materia, CSIC, Serrano 119, 28006 Madrid, Spain
E. LÓPEZ CABARCOS, H. G. ZACHMANN
Institut für Technische und Makromolekulare Chemie, Universität Hamburg, Hamburg, FRG
A. PAULSEN, F. BRÜNING, W. MEINS
Fachhochschule Harburg, Hamburg, FRG

In Parts 1 and 2 of this series the influence of mould geometry and processing parameters was investigated for elongational flow injection moulded polyethylene with the aim of improving the mechanical properties. In the present study (Part 3) injection moulding of commercial polyethylene samples has been carried out using a wide range of molecular weights. Two moulds were used, one of them only providing shear flow, the other one allowing, in addition large elongational flow. In the case of the mould with large elongational flow, at a critical molecular weight, which depends on the melt temperature, a well defined transition in birefringence and mechanical properties of the injection mouldings has been detected. This transition has been discussed in terms of a development of a percolating network structure of long-lived stable knots yielding high mechanical strength oriented mouldings.

1. Introduction

Polymer orientation from injection moulding usually is a complex superposition of shear deformation and elongation [1]. Conventional moulds mainly provide shear flow in narrow channels and areas close to the cavity walls, where the melt is stretched. By adequately modifying the geometry of the flow-channel (conical cross-section) a large axial elongational flow component has been additionally introduced [2–3]. "Elongational flow injection moulding" follows the basic experiments of Keller and Odell [4] aimed at improving polymer strength through combination of flow-induced high molecular orientation and pressure within a capillary. The orientation within the injection moulded material is often inhomogeneous, elongational flow developing mainly in the centre and shearing deformation zones arising in the vicinity of the cavity walls. The morphology of the injection moulded material has been shown to be one of interlocking shish-kebabs, with the layer normals oriented along the injection direction [5]. Correlations between orientation and mechanical properties (modulus, yield strength, etc.) for the injection moulded material are well established.

In Parts 1 and 2 of this series [6, 7] the influence of the mould geometry and the processing parameters upon the properties of injection mouldings was discussed in detail for a mould cavity which provided elongational flow during the filling process. In the present study the properties of polyethylene materials processed using two moulds, one providing shear flow and the other one giving large elongational flow in addition, have been compared. A series of commercial polyethylenes has been used in order to study the influence of the molecular weight of different materials on the tensile mechanical properties. In this investigation mainly linear polyethylenes were selected though, additionally, a few samples containing a low level of side branches were also studied. The conspicuous strong increase in mechanical properties found beyond a critical average molecular length will be brought out as the main result of the present study. An attempt to discuss this finding in terms of a development of a percolating network of long-lived stable entanglements will be presented.

2. Materials and techniques

Table I shows the melt flow index (MFI), the viscosity average molecular weight M_η, the number, M_n, and weight average, molecular weight, M_w, and the density of the materials investigated. While M_n, M_w and the melt indices were specified by the manufacturers the other quantities were measured in our laboratory.

Injection moulding experiments were carried out using first, a two-arm mould allowing elongational flow as described in [1] (Part I) and, second, a "conventional" mould with a larger cross-section than the inlet. Fig. 1 shows the shape of the conventional mould and the dimensions of the moulding. The melt temperatures, T_m, were varied while keeping the other

Permanent address: Institut für Technische und Makromolekulare Chemie, Universität Hamburg, Hamburg, FRG.

0022–2461/89 $03.00 + .12

TABLE I PE materials investigated

Commercial name	MFI (2.16 kg)	MFI (21.6 kg)	M_η	M_w	M_n	ϱ (g cm^{-3})	log M_η
Vestolen A 6017	11		51 134	51 000	5 500	0.966	4.709
Lupolen 6031 M	7		52 270	73 373	16 562	0.966	4.718
Hostalen GC 7260	8		55 204	68 000	13 000	0.959	4.742
Vestolen A 6016	7		56 212	58 000	7 100	0.966	4.750
Vestolen A 6014	3.5		74 799	71 000	11 000	0.958	4.874
Vestolen A 6013	2		88 225	80 000	12 100	0.970	4.946
Vestolen A 6012	0.8		113 322	108 000	11 900	0.959	5.054
Rigidex 6006-60	0.6		114 838			0.962	5.060
Lupolen 6021 D	0.2		161 133	182 527	25 273	0.962	5.207
Lupolen 5661 B		9	173 210			0.959	5.239
Lupolen 4261 A		6.1	201 345			0.947	5.304
Marlex 56020		2.5	226 046			0.952	5.354
Lupolen 5261 Z		2.0	247 750	477 982	39 120	0.958	5.394
Hostalen GB 7255		1.8	276 938			0.952	5.442
Hostalen GB 6255		1.5	307 080			0.985	5.487

processing parameters constant. Table II gives the selected processing parameters. In the case of the elongational-flow mould, melt temperatures of T_m = 148° C and 210° C were used. With the conventional mould, owing to the need to use a smaller die (smaller inlet cross-section), T_m = 148° C could not be adjusted because of increased frictional heat. Therefore, in this case melt temperatures of 185° C and 250° C were employed.

Tensile tests were carried out using a Zwick machine with a cross-head speed of 20 mm min^{-1}. Notches were machined in the centre of the moulds for the high strength bars, the tenacity of which, otherwise, could not be measured due to destruction of the samples at the clamps. Birefringence profiles across the 4 mm diameter thickness of the bars (Fig. 1a) were obtained from microtomed cuts. Fig. 2 shows the geometry of the cut for the normal injection mould in the *xz* plane. Similar 4 mm-thick microtomed cuts were also taken from the elongational-flow injected bars, though now, in the *xy* plane as described in Part 2 [7]. Birefringence was measured using crossed polarizers and a calcite compensator. Density was determined, using an isopropanol-dioxane density gradient column. To characterize the molecular weight of the materials, viscosimetric measurements of diluted decalin solutions at 135° C were carried out.

3. Results

3.1. Characterization of the materials

Fig. 3 shows the correlation found between melt index and log M_η. From these data it is seen that the quantity M_η can be considered as a good measure for the flow characteristics of the injected materials.

Molecular irregularities like chain branching, unsaturations and large differences in the distribution of chain lengths are hindering the crystallization from the melt. The density of materials crystallized under the same conditions offers, in principle, a measure of the level of chain irregularities. Fig. 4 shows the density of the materials investigated in the present study as a function of log M_η. For some of the samples investigated (full symbols) the density linearly decreases with increasing logarithm of molecular weight irrespectively of the mould type used. A similar decrease has been reported by other authors [8]. The data obtained for the rest of the samples (open symbols) deviate, however, substantially from the linear decrease. We attribute this deviation to different defect concentrations. From the relation between density and branching content reported by Rueda and Baltá-Calleja [9] it turns out that the linear polyethylene samples that crystallize well have a branching concentration smaller than 0.2 defects per 10^2 carbon atoms. The estimated number of chain defects per 100 carbon atoms for the worst crystallizing materials lies

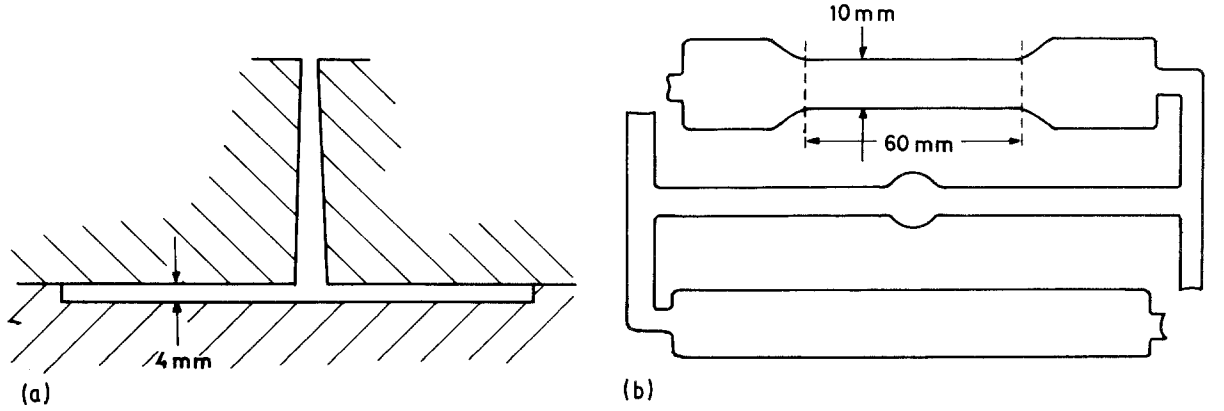

Figure 1 "Normal Mould" cross-section of inlet and mould-halves. (a) View as seen edge on. (b) Projection at 90° to (a). The upper part of the mould was cut and used for the tensile tests.

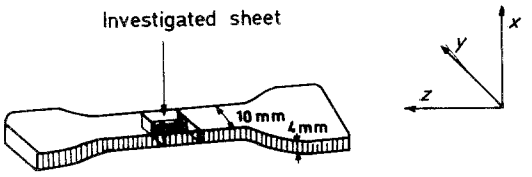

Figure 2 Schematic drawing of a 40 μm thick microtomed cut from the centre of the normal injection moulding used for birefringence measurements.

between 0.3 to 0.8 chain defects per 100 chain atoms (Table III). We can, thus, classify the investigated materials in samples that crystallize well, following a logarithmic molecular weight decreasing dependence, and defective crystallizing materials with depressed density values, due to the presence of chain defects.

3.2. Birefringence profiles

Fig. 5 shows typical birefringence profiles of samples obtained by means of *conventional injection moulding*. Birefringence profiles of two representative materials, a low-(left) and a high-molecular weight grade (right) are respectively shown for two melt temperatures. Birefringence, Δn, is here plotted as a function of x (see Fig. 2). As expected, high birefringence values are observed near to the walls where the shear velocity is comparatively large. In the centre of the cross-section, due to the decrease of shear velocity and the higher melt temperature used, low birefringence values are observed. The maximum values of birefringence notably increase with molecular weight for both processing (melt) temperatures. The influence of melt temperature on birefringence is, however, relatively small.

Fig. 6 illustrates the corresponding birefringence profiles for the two above materials using the *elongational flow mould*. In this case, besides the shear zones of high birefringence near the walls, distinct birefringence maxima emerge in the central part of the cross-section. As discussed earlier [6] these maxima are due to the elongational flow. The elongational induced birefringence increases strongly with molecular weight (Figs 6b and d) and decreases with processing temperature (Figs 6a and b). It is to be noted that the effects of molecular weight and processing temperature are much more pronounced on elongational flow induced birefringence than on shear flow induced birefringence (Fig. 5). In the case of the high molecular weight material processed at low temperatures (Fig. 6c), both, shear zones and elongational flow zones merge.

The birefringence maxima in the *shear zone*, Δn_s^{max}, (normal mould) are plotted in Fig. 7 as a function of M_n for both moulds. Fig. 8 shows the corresponding

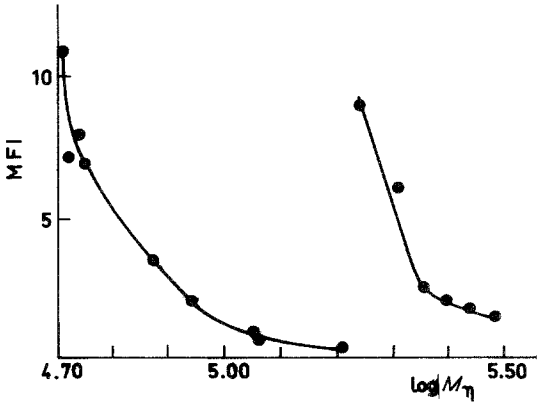

Figure 3 Plot of melt flow index (MFI) against log M_η. Large MFI changes were measured with a weight of 2.16 kg (left). Small MFI changes above $M_\eta = 10^5$ were determined using 21.6 kg (right). Testing temperature 190° C.

results for the maximum birefringence, Δn_e^{max}, in the *elongational flow zone*.

For the normal mould a nearly constant maximum birefringence in the shear zones is observed at the low molecular weights followed by a steep increase at a critical molecular weight, M_c, which depends on T_m (Fig. 7a). In contrast, for the elongational-flow mould a large decrease of Δn_s^{max} with increasing molecular weight is observed before M_c is reached (Fig. 7b). Table IV summarizes the critical molecular weights observed for different mould types and melt temperatures. Here it is shown that M_c increases with melt temperature and is larger for the elongational flow mould.

The maximum birefringence values obtained for the elongational flow component (Fig. 8) in the case of $T_m = 210°$ C confirm the transition found in case of the shear zone at $M_c \approx 115.000$. However, in case of the moulds processed at $T_m = 148°$ C no such transition is found due to the fact that below $M_n = 115.000$ the profiles are strongly fissured showing already the same maximum value as detected above M_c. Figs 6c and d provide illustrative examples for the difference of profiles below and above the transition at $M_c \approx 115.000$, and $T_m = 148°$ C, for the elongational flow mould. In this case fissures specially appear in the central elongational zone.

Fig. 9 illustrates the plot of the mean birefringence, $\overline{\Delta n}$, averaged over the sample cross-section against the molecular weight for the elongational-flow injection moulds processed at $T_m = 210°$ C. The step-like transition in $\overline{\Delta n}$ is most distinctly observed at high processing temperatures. For $T_m = 148°$ C the scattering of data does not yield such a well defined transition. The slight decreasing tendency of the birefringence

TABLE II Injection parameters

Mould temperature	20° C
Injection pressure	200 MPa
Nominal pressure on solidifying melt	200 MPa
Time of applied pressure	60 sec
Revolutions per minute of the screw	90 min^{-1}
Injection speed	3.5 mm sec^{-1}

TABLE III Number of chain defects for the worse crystallizing materials (defects per 100 carbon atoms)

Hostalen GC 7260	0.3
Vestolen A 6014	0.4
Vestolen A 6012	0.3
Lupolen 4261 A	0.8
Marlex 56020	0.6
Hostalen GB 7255	0.6

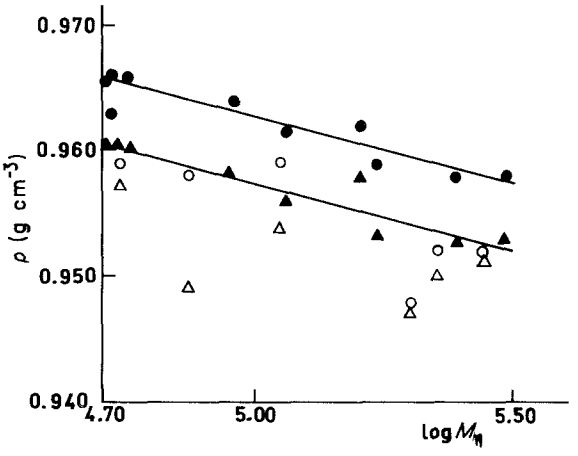

Figure 4 Plot of density as a function of log M_η. Upper curve: Compression moulded samples at T_m = 150° C. Cooling speed ≈ 4° C min^{-1}. Lower curve: Elongational flow injected mouldings at T_m = 148° C. Open symbols indicate bad crystallizing materials (Table III).

at elevated molecular weights (Figs 7 to 9) can be correlated to the influence of the material entering the mould, showing a rubber-like behaviour at these high M_η values, thus, sliding along the walls of the cavity. This mechanism does not contribute to orientation and is competing with the shear flow contribution yielding orientation near the cavity walls. For the normal mouldings the transition in $\overline{\Delta n}$ is obscured due to the increase of the width of the shear zones leading to an additional increase of $\overline{\Delta n}$ above M_c.

3.3. Mechanical properties

Fig. 10 shows the mechanical strength, σ, of the processed bars as a function of log M_η. It clearly evidences the great difference in σ between elongational flow and normal moulds. A direct consequence of the high orientations occurring in the elongational-flow zone, is that the strength of the elongational-flow injection mouldings is notably higher than that of the conventional injection materials. The slight decrease in birefringence on the high molecular weight region of Figs 7 to 9 is reflected in a parallel decrease of mechanical strength shown in the curves of Fig. 10. Characteristic low birefringence values due to the presence of chain defects (see Table III) similarly yield depressed values of mechanical strength.

Most interesting is the result that the abrupt transition in birefrinence obtained at M_c for the elongational flow injection moulded bars is paralleled by a conspicuous increase in the mechanical strength. This even applies to the lower temperature of T_m = 148° C, where the birefringence transition is not so pronounced. The σ value for the normal injection mouldings (lower curves in Fig. 10) does not show, on the contrary, such a well defined discontinuous behaviour. The σ values in this case lie in the vicinity of 28 MPa, corresponding to the strength of unoriented crystalline polyethylene. Here, the influence of the thin shear zones on the mechanical strength is not effective on the overall strength of the injection moulding.

Fig. 11 illustrates the mechanical strength data plotted against the averaged birefringence $\overline{\Delta n}$. The low

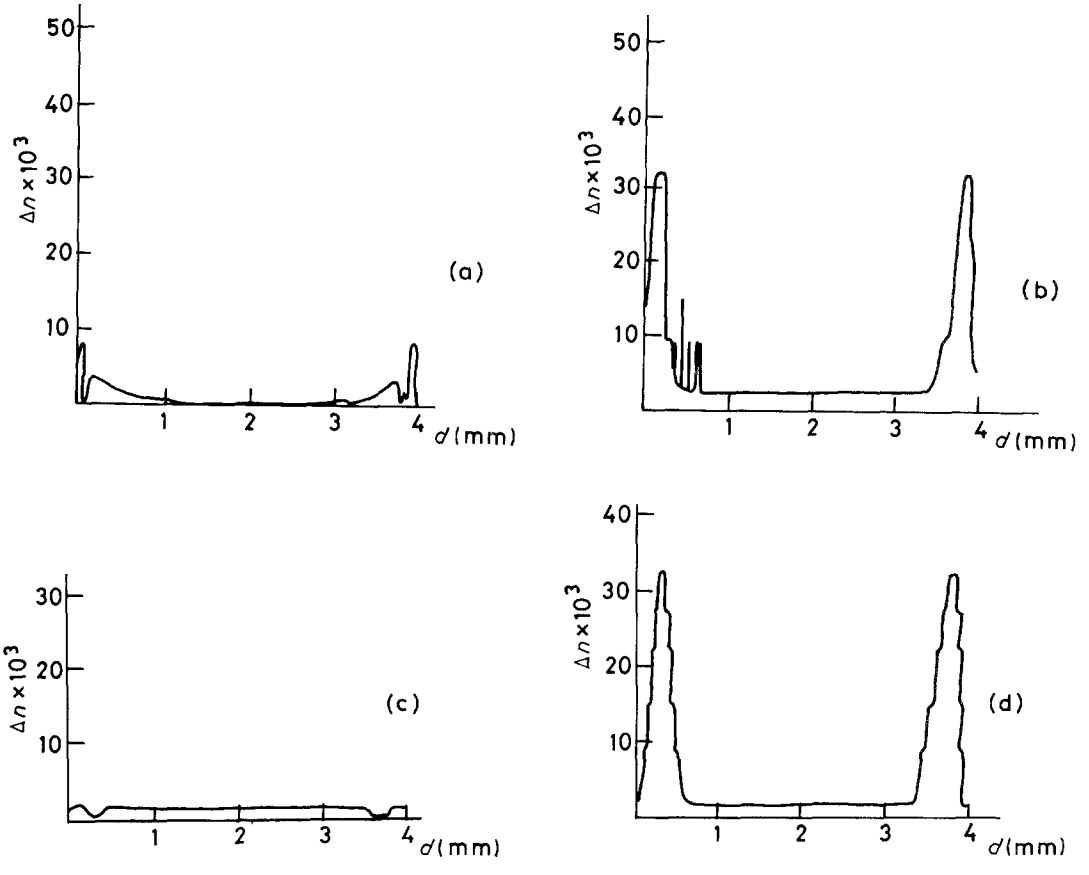

Figure 5 Birefringence profiles across the thickness of an injection moulding measured in the x direction (see Fig. 2) in the middle of the sample. Normal injection mould: (a) (T_m = 250° C, M_η = 52 270), (b) (T_m = 250° C, M_η = 161 133); (c) (T_m = 185° C, M_η = 52 270) (d) (T_m = 185° C, M_η = 161 133).

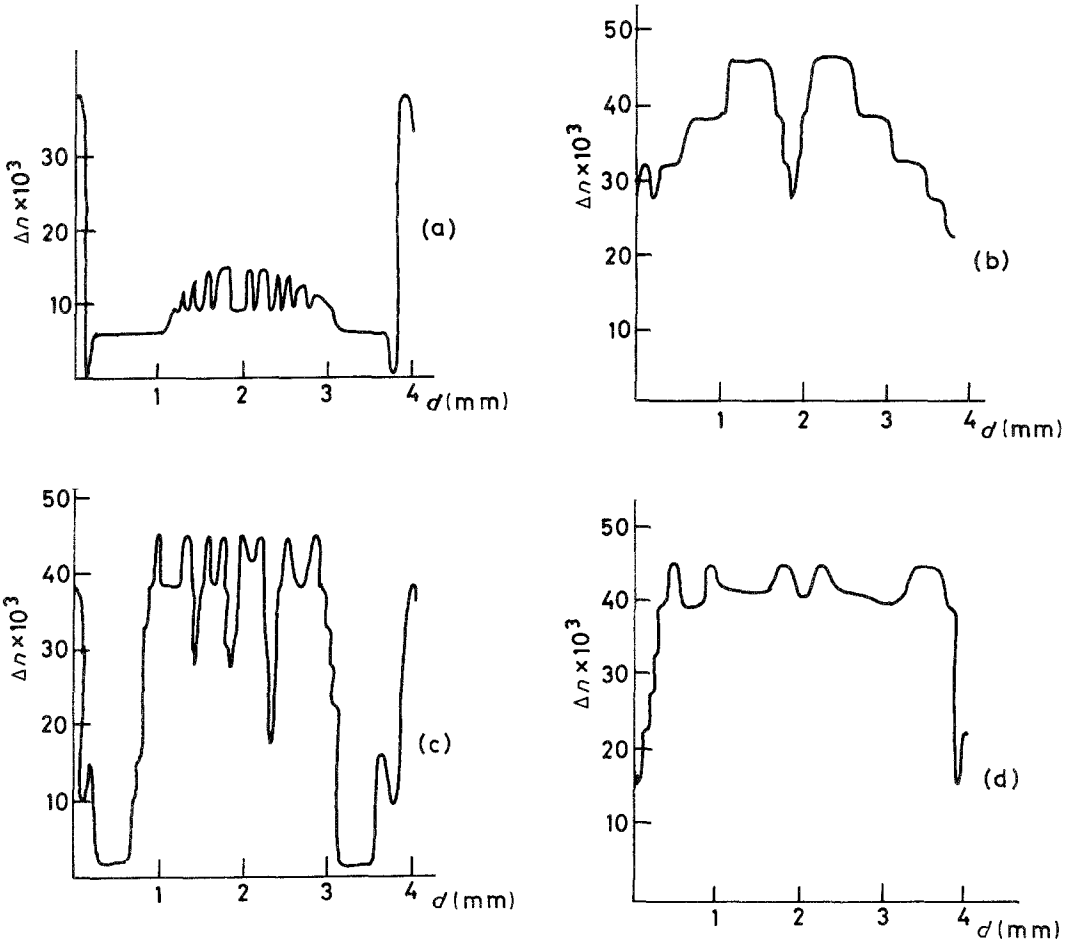

Figure 6 Birefringence profiles measured along the y axis for the elongational flow mould: (a) (T_m = 210° C, M_η = 52 270), (b) (T_m = 210° C, M_η = 161 133), (c) (T_m = 148° C, M_η = 52 270; (d) (T_m = 148° C, M_η = 161 133).

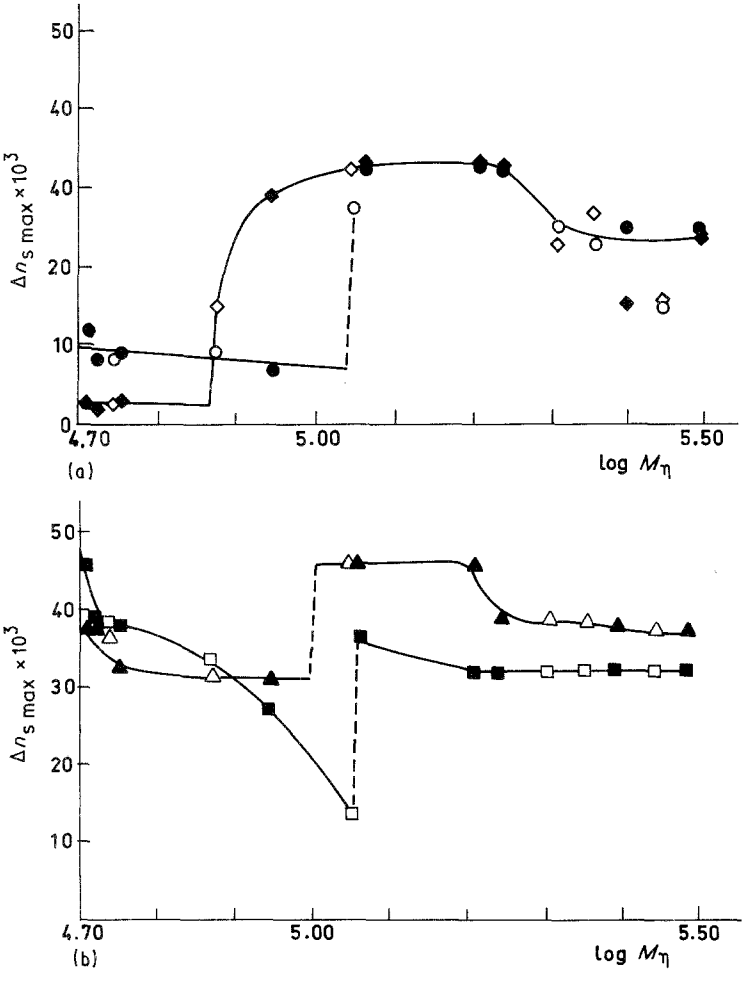

Figure 7 Maximum birefringence values at the shear zones of profiles as a function of log M_η (see Fig. 5). (a) Normal mould: ◆ T_m = 185° C, ● T_m = 250° C. (b) Elongational flow mould: ▲ T_m = 148° C, ■ T_m = 210° C. Open symbols represent worst crystallizing material.

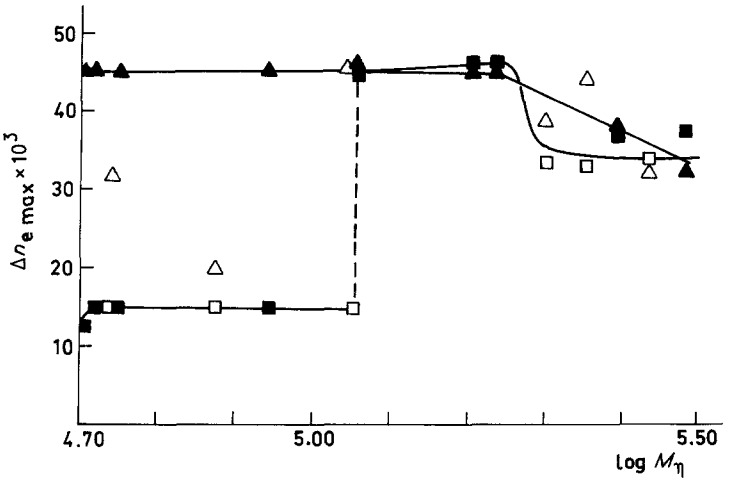

Figure 8 Maximum birefringence values in the elongational flow zone (elongational flow mould) as a function of M_η. Parameter: T_m. Symbols as in Fig. 7b.

orientation zone (left) corresponds to the normal injection moulding procedure. It is seen that the data points representing the results obtained with the normal moulding overlap with the points representing the results obtained with the elongational flow mould. Values of $\overline{\Delta n} > 15 \times 10^{-3}$ are obtained only with elongational flow injection moulding. For $T_m = 210°$ C a linear variation of σ with $\overline{\Delta n}$ is obtained. For $T_m = 148°$ C the same linear increase is followed up to a birefringence of $\overline{\Delta n} \sim 40 \times 10^{-3}$. However, at $\overline{\Delta n} \sim 30 \times 10^{-3}$ a sudden transition takes place. This critical value of $\overline{\Delta n}$ corresponds to the critical molecular weight M_c shown in Fig. 10. Beyond the critical molecular weight the mechanical strength of elongational flow injected samples at low processing temperature no longer fits the linear σ–$\overline{\Delta n}$ plot. Despite having comparable mean birefringence values, the σ data for $M_n > M_c$ lie considerable higher. In Part 2 (Fig. 13) the gradual transition between these two extremes was attained by varying continuously the processing temperature and pressure of a material above M_c. This underlines the much sharper transition in mechanical strength than in birefringence as observed for the low processing temperature series. Thus, above M_c one may infer the onset of a special structural mechanism at high $\overline{\Delta n}$ values, correlated to the large σ increase. At high processing temperatures ($T_m = 210°$ C) two of the high molecular weight specimens of the elongational flow mould series also deviate to high σ values. Presumably a similar structural effect, to be discussed below, also influences in this case the strength of these samples.

Figs 12 and 13 show the elongation at break of the bars obtained from tensile tests. The above transitions of birefringence and mechanical strength at M_c correspond here to a transition from ductile to brittle fracture. At low molecular weights all the bars are ductile except for the series produced at low processing temperature by the elongational flow mould (Fig. 4). The ductile bars exhibit a necking zone which propagates at further deformations. This transition occurs most distinctly in the case of the high-temperature elongational-flow injection-mouldings (Fig. 12). Highly oriented samples above the transition are brittle. In this case fracture occurs at a deformation of 30 to 40%, when the bars start forming the neck.

While the birefringence transition is not followed by a parallel clear transition in σ for the normal injection mouldings shown in Fig. 10, the data of elongation at break given in Fig. 12 show clearly this effect. The shift of the critical transition due to the processing temperature is also confirmed in Fig. 12. However, the decreasing of elongation at break with increasing M_η in the low molecular weight region does not correlate to the observed near constancy of the birefringence maxima in this region (Fig. 7a). This discrepancy between ε_b and Δn will be discussed in Section 4. It is, further, noteworthy that, for normal injection mouldings the mechanical strength is related to the inner part of the mould, whereas the elongation at break is here strongly correlated to the orientations in the outer zones. This was confirmed by removing the oriented outer skin (0.4 mm) (elongation at break ~40%) of a bar which normally exhibits a brittle behaviour (log $M_\eta = 5.054$, $T_m = 185°$) showing

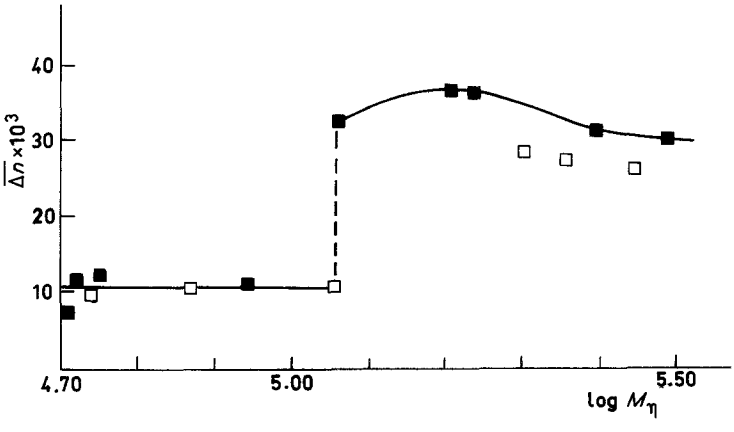

Figure 9 Averaged birefringence as a function of log M_η for the elongational flow mould. Symbols as in Fig. 7.

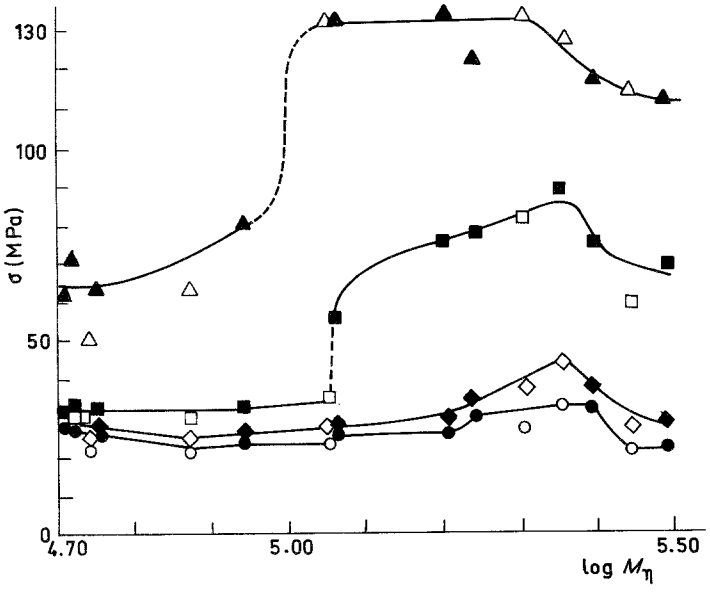

Figure 10 Plot of mechanical strength of injection moulded PE-bars as a function of log M_η. Symbols as in Fig. 7.

that after peeling off the sample ductile behaviour is found again (elongation at break: ~600%).

3.4. Density measurements

Fig. 14 shows the plot of reduced density $\varrho/\varrho_{\text{normal-mould}}$ (T_m = 250° C) as a function of log M_η illustrating the influence of mould geometry and injection temperature. Thus, density is larger for elongational flow injection moulding than for the normal injection mouldings. On the other hand, density decreases with decreasing T_m. Generally, high densities are correlated to high birefringence values, i.e. the highest densities and birefringence values are obtained in case of elongational flow injection moulding at low temperature (148° C). The influence of molecular weight and chain perfection, as well as the transitions at M_c are included in the ϱ values of the normal injection mouldings at T_m = 250° C, with respect to which the other density values have been normalized, and should not appreciably affect the data of Fig. 14. Straight horizontal lines are, hence, obtained for the reduced ϱ values of normal mouldings and for the elongational flow moulding using, T_m = 148° C. Only in the case of the elongational flow mould with T_m = 210° C a pronounced ϱ transition at M_c, which parallels to that seen in $\overline{\Delta n}$ (Fig. 9), can be observed.

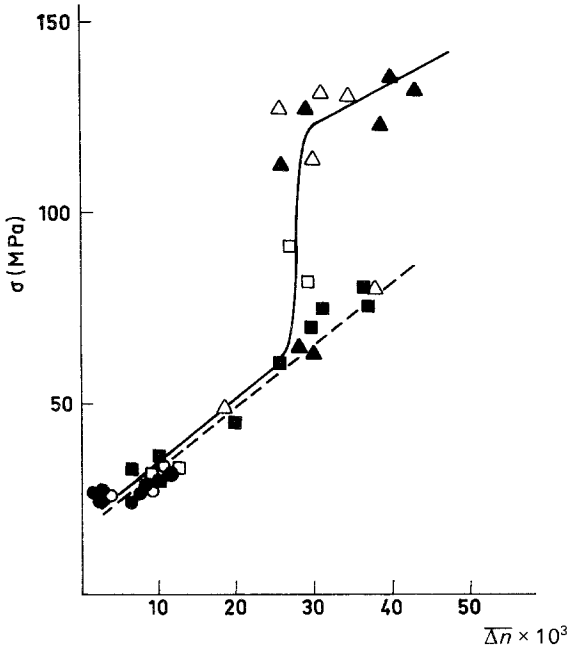

Figure 11 Plot of mechanical strength against averaged birefringence. Symbols as in Fig. 7.

3.5. Influence of pressure

In Part 2 [2] it was shown that the applied pressure on the solidifying melt, within the mould, directly affected the birefringence, mechanical strength and density of the mouldings. Within this context it is convenient to point out that the influence of pressure throughout the transition range of properties is negligible. Indeed, pressure in the mould does not show-up any substantial changes throughout the region of the critical molecular weights as evinced in Part 2 [2]. High pressure induces an increase of birefringence due to a quick preservation mechanism of the flow induced orientation by pressure induced crystallization. According to the data of [2] a slightly higher orientation should be expected, especially in the low molecular weight region. In the low molecular weight region birefringence profiles (Fig. 6c) are, however, more fissured than above M_c (Fig. 6d). Therefore, pressure cannot explain the high orientation observed above M_c. Such a high orientation due to the flow history of the filling process will be discussed in the following section.

4. Discussion

4.1. Transition of properties at a critical molecular weight and formation of a network of stable knots

The above results indicate that when the molecular chains reach a longer length than that of the critical molecular weight, M_c, then the values of σ and Δn rise notably and a transition of the material from ductile to brittle behaviour is obtained. In glassy polymers one observes a similar stepwise increase of the fracture energy with increasing molecular weight which has been related to the presence of chain entanglements

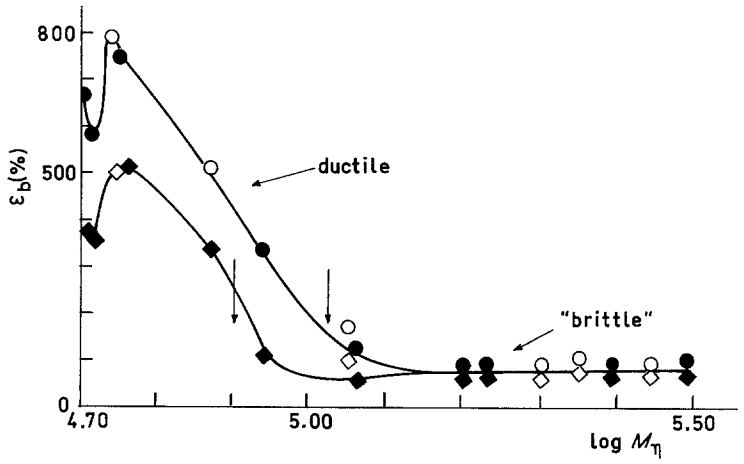

Figure 12 Elongation at break of polyethylene injection moulded bars (normal mould) against log M_η. Parameter: T_m. Arrows indicate the transition form ductile to brittle behaviour. Symbols as in Fig. 7a.

[10]. It is well known that molten polymers are entangled if the molecular weight is greater than a critical value [11–15]. A well known example is the marked increase in the molecular weight dependence of viscosity above a critical value M_c. Entanglements between molecular segments can be visualized as temporary physical coupling points liable of transmitting mechanical stresses [16]. The cross-over and backfolding of two segments or the intimate contact of two kinked segments are the most often used interpretations. Tight molecular knots, involving two or more chains, are expected to be a very stable kind of entanglements and have been proposed by de Gennes to account for long relaxation times [16]. Tight knots have also been discussed to describe the behaviour of polymer melts under strong shear flow [18, 19].

Since injection moulding involves mass transport from the melt through flow-induced molecular orientation into the mould it is convenient to analyse the mechanical properties of the mouldings in the light of the properties of the melt itself. The rheological properties of the melt have been described by Lodge in terms of a fluctuating network model [20]. The parallelism between the mechanical properties of the melt (elastic recovery and elongation at break) and those of solid melt-spun monofilaments has been attributed by Bayer [21, 22] to the long-lived component of these entanglements (to be called stable knots). From this parallelism it is inferred that stable knots survive the production process from the melt into the solid state [21, 22]. In what follows we shall invoke the concept of stable knots to explain the measured properties of the injection mouldings.

The observed transitions of birefringence, mechanical strength and elongation at break reported in the present work can be discussed in terms of a physical network of mainly long-lived stable entanglements (chain knots) which is developing beyond a critical length M_c. We have suggested elsewhere [21, 22] that the extension of such a network of stable knots increases with increasing molecular weight and with decreasing melt temperature. Such a behaviour is consistent with the observed shift, near M_c, of the Δn transition towards low M_η values with decreasing melt temperature, evinced for both mould geometries (Figs 7 to 9). Only at such a critical length the molecules can form a coherently stable network that describes the observed transition. Thus, at low T_m values the critical molecular length is observed at lower molecular weights while at high T_m values M_c is found at higher molecular weights (see Table IV). The shift of the Δn transition due to variation of mould geometry may be explained in the same manner: the normal mould (Fig. 2) undergoes a much stronger cooling of the melt before entering the bar shaped part of the mould than the elongational flow mould. This is due to the shorter path of the melt in the latter case. Thus, one can assume an effective lower melt temperature in the shear zones of the normal mould, so that the T_m value for the Δn transition is lower for the normal mould (Fig. 7a) than for the elongational-flow mould (Fig. 7b).

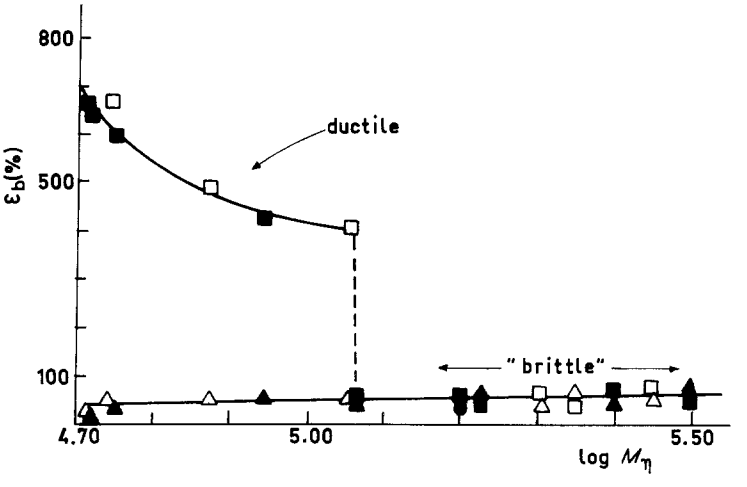

Figure 13 Elongation at break for mouldings which were processed by the elongational flow injection method. Symbols as in Fig. 7b.

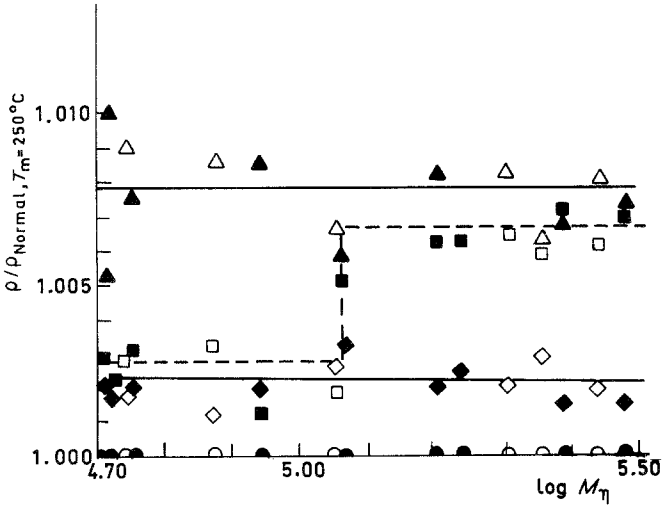

Figure 14 Reduced plot of density of PE-injection mouldings plotted against log M_η. Values are referred to the density of normal mouldings processed at T_m = 250° C. Symbols as in Fig. 7.

A possible way to describe the critical molecular weights, M_c, reported in this study is through a "percolation" mechanism of long-lived knots linking adjacent coils and extending through the material to build-up a three-dimensional network. With the gradual development of such a network of stable knots increasingly larger stresses can be transmitted to chain molecules in shear or in tension. The critical molecular weights collected in Table IV, underlying the Δn and σ transitions, lie within the same range as those derived from measurements of elastic recovery [21, 22], supporting the development of the supernetwork at M_c.

4.2. Relation between Δn and ε_b

In general large values of Δn correspond to small values of ε_b (brittle material) and small values of Δn correspond to larger values of ε_b (ductile materials). Below the percolation threshold one observes, however, that the ε_b data (Fig. 12) for the normal mouldings do not show any correlation with the Δn results (Fig. 7), suggesting that the variation of ε_b with M_η must have a different origin than simply chain orientation. According to the foregoing arguments, high values of ε_b below M_c would suggest the presence of a poorly developed network structure of molecular knots allowing high deformations before fracture occurs. On the contrary, above M_c, the formation of a network leads to high Δn values only allowing small plastic deformation of the material before fracture sets up, resulting in the brittle behaviour observed above M_c in Fig. 12. According to Table IV the network develops with decreasing T_m and increasing M_η. Hence, the observed increase of ε_b in the low M_η region and the larger values obtained at higher T_m (Figs 12 and 13) could be correlated to a poorer network development.

TABLE IV Critical molecular weight, M_c, as derived from the maximum birefringence at shear zones in Fig. 7.

Mould	T_m (° C)	M_c
normal	250	110 000
normal	185	60 000
elongational	115	115 000
elongational	148	100 000

4.3. Dependence of σ on Δn and shish formation

The conspicuous stepwise increase of σ with Δn, deviating from the linear behaviour (see Fig. 11), for the elongational-flow injection mouldings can be correlated to the formation of a very great number of shish-kebab crystals beyond M_c [23]. The presence of shish-kebab crystals is, admittedly, related to high molecular orientation values [4]. Shish formation leads to a reinforcement of the material and, thus, to an additional increase of σ. The fibrous precursors of extended-chain crystals formed by the extensional flow field act as nuclei causing an increase of the onset of the crystallization temperature, inducing, as a result, an increase of crystallinity [24]. This could explain the observed increase of density of the elongational flow-injection mouldings above M_c at 210° C (Fig. 14).

Shish formation from a melt network structure has been discussed by Bayer *et al.* [7] in the light of shrinkage measurements at 170° C and birefringence on elongational flow injection moulded bars at room temperature. Here it was shown that at low T_m values shrinkage decreases and birefringence concurrently increases. This unexpected effect was attributed to a plastic deformation of the network by a slipping process of active knots sliding along taut molecules

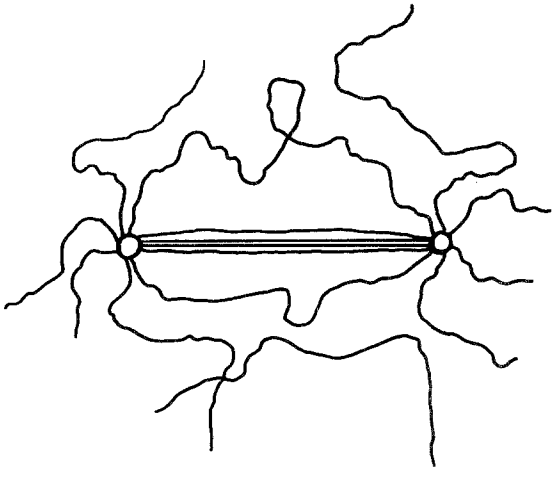

Figure 15 Schematic representation of the formation of a shish in the melt by extension of narrow meshes and concurrent sliding of active knots along taut strained molecules.

within deformed meshes. Thus, the joint formation of taut strained molecules upon deformation of the injected melt and the slippage of the remaining active knots during this process can be visualized as closely related effects. Bundles of taut molecules preferentially in zones of narrow meshes may, hence, explain the formation of shishs (see Fig. 15). In summary, this process offers a model of deformation for the oriented materials and justifies the results of Fig. 11, emphasizing the relevance of the network structure to explain the σ transition above M_c.

5. Conclusions

The results obtained with elongational-flow injection moulded polyethylene processed at high temperature show-up a pronounced increase of birefringence, mechanical properties and density at a critical molecular weight of about $M_c \sim 10^5$. From the above results it is concluded that this step-wise transition can be related to a development of a coherent network of stable knots which are transferred from the melt into the oriented solid state, leading to enhanced mechanical strength values.

Acknowledgements

The authors wish to express their thanks to the Internationales Büro, Kernforschungsanlage, Karlsruhe and M^0 Asuntos Exteriores, Madrid, for the generous support of this cooperation project. One of the authors (R.K.B.) also wishes to acknowledge the DFG (FRG) for a grant during his stay in Hamburg and to CAICYT (Spain) for the tenure of a sabbatical grant during his work in Madrid. Thanks are due to R. Dieckow and P. Wiegel, Laboratorium für Kunststofftechnik of the Fachhochschule Hamburg for their valuable help with the injection moulding machine.

References

1. F. JOHANNABER, "Injection Moulding Machines" (Hanser Verlag, München, 1985).
2. R. K. BAYER, Europhysics Conference Abstracts, 14th Europhysics Conference on Macromolecular Physics, Vilafranca del Penedes, Vol. 69, edited by W. J. Merz, (European Physical Society, Zurich, 1982) p. 75.
3. R. K. BAYER, A. E. ELIAH and J. C. SEFERIS, *Polym. Eng. Rev.* **4** (1984) 201.
4. J. A. ODELL, D. I. GRUBB and A. KELLER, *Polymer* **19** (1978) 617.
5. W. HECKMANN, PhD Thesis, TH Darmstadt (1976).
6. R. K. BAYER, F. J. BALTÁ CALLEJA, H. G. ZACHMANN and U. UMBACH, *Polym. Eng. Sci.* (Part I) **29** (1989) 186.
7. E. LÓPEZ CABARCOS, H. G. ZACHMANN, R. K. BAYER, F. J. BALTÁ CALLEJA and W. MEINS, *Polym. Eng. Sci.* (Part II) **29** (1989) 193.
8. J. MAXFIELD and L. MANDELKERN, *J. Phys. Chem.* **69** (1964) 417.
9. D. R. RUEDA, F. J. BALTÁ-CALLEJA and A. HIDALGO, *Opt. Pure. Appl.* **11** (1978) 67.
10. H. H. KAUSCH and K. JUD, *Plast. Rubber Processing Appl.* **2** (1982) 265.
11. R. S. PORTER and J. F. JOHNSON, *Chem. Rev.* **66** (1966) 1.
12. J. D. FERRY, "Viscoelastic Properties of Polymers" 2nd Edn (Wiley, New York, 1980).
13. W. GRAESSLEY, *Adv. Polym. Sci.*, **16** (1974) 1.
14. *Idem., ibid,* **47** (1982) 67.
15. J. RAULT, *J. Non-Newtonian Fluid Mech.* **23** (1987) 229.
16. H. H. KAUSCH and M. DETTENMAIER, *Colloid Polym. Sci.* **260** (1982) 120.
17. P. G. DE GENNES, *Macromolecules* **17** (1984) 703.
18. M. MACKLEY and A. KELLER, *Phil. Trans. R. Soc. London* **278** (1975) 29.
19. F. C. FRANK and M. MACKLEY, *J. Polym. Sci.* **14** (1976) 1121.
20. A. S. LODGE, "Elastic Liquids", (Academic Press, London, 1964).
21. R. K. BAYER, *Rheol. Acta* (in press).
22. R. K. BAYER, F. LIEBENTRAUT and T. MEYER, *Rheol. Acta* (in press).
23. W. HECKMANN, Private Communication.
24. J. E. SPRUIELL and J. L. WHITE, *Polym. Eng. Sci.* **15** (1975) 660.

Received 1 June
and accepted 13 September 1988